Scholar Publishing Group
International Journal of Engineering Technology and Construction
https://doi.org/10.38007/IJETC.2025.060113
ISSN 2789-7176 Vol. 6, Issue 1: 130-140

Influence of Pile Length on Performance of Prestressed Geosynthetic-Reinforced Sheet Pile Walls via Model Tests

Yong Liu[1,a], Zhilong Shi[1,b], Tengfei Yan[2,3,c*]

[1]*China Railway Eryuan Chongqing Survey and Design Institute Co., Ltd., Chongqing 401120, China*

[2]*School of Civil Engineering, Southwest Jiaotong University, Chengdu 610031, China*

[3]*No.1 Jiaxing Hospital, Jiaxing 314000, China*

[a]*email: 804281078@qq.com,* [b]*email: shizhilong1984@163.com,* [c]*email: 961757098@qq.com*

**Corresponding author*

Keywords: Prestressing; Geosynthetic reinforcement; Sheet pile retaining wall; Bearing capacity; Railway embankment

Abstract: Prestressed geosynthetic-reinforced sheet pile retaining walls are increasingly considered for railway applications requiring enhanced load-bearing performance and deformation control. This study investigates the effects of prestress and pile length on the structural response of such composite walls through two sets of scaled indoor model tests. Load–settlement behavior, horizontal displacement, bending moments, reinforcement strains, and earth pressure distributions were measured under pre-prestressed and post-prestressed loading conditions. Results indicate that prestressing significantly increases ultimate bearing capacity, enhances soil–reinforcement interaction, and reduces lateral displacement. Shorter piles exhibit lower bearing capacity, higher horizontal displacement, and increased reinforcement strain due to reduced anchorage and weaker soil restraint. Bending moment distributions follow a parabolic pattern, with prestressing amplifying peak moments and strains, particularly in short-pile configurations. The findings provide experimental evidence for the design and optimization of prestressed geosynthetic-reinforced sheet pile walls in railway engineering, offering insights into their load transfer and deformation mechanisms.

1. Introduction

Sheet pile retaining walls are widely used in railway engineering for track widening, embankment protection, foundation stabilization, and disaster mitigation along constrained corridors [1-3]. Owing to their modularity, rapid construction, and low disturbance to existing lines, they have become a key structural form for modern railway upgrading and reconstruction projects [4-6]. Traditional sheet pile retaining walls, however, often suffer from insufficient lateral stiffness, pronounced deformation under high train loads, and limited resistance to long-term environmental

actions. With the continuous increase in axle load, train speed, and service performance requirements, these limitations have become a critical technical bottleneck. Consequently, enhancing the bearing capacity, deformation control, and service resilience of sheet pile retaining walls has become an urgent engineering challenge in railway geotechnics.

Geosynthetic reinforcement technology has been extensively applied in retaining structures, embankment subgrades, and slope stabilization, supported by a well-established body of research on its tensile reinforcement effect, separation function, and restraint mechanism [7-9]. In recent years, the introduction of "prestress" into geosynthetic-reinforced soil systems—through compaction-induced tension, preloading, or controlled deformation during construction—has emerged as an effective method to improve structural stiffness, enhance soil–geosynthetic interaction, and mitigate early-stage deformation [10-12]. Prestressing allows the reinforcement to mobilize tensile capacity at small strains, thereby providing faster structural response, improved load distribution, and better control of wall deflection [13-14]. Although these concepts have been explored in reinforced soil retaining walls and reinforced backfills, the mechanisms governing the mobilization, transfer, and long-term effects of prestress within railway sheet pile retaining wall systems remain insufficiently understood. Specific questions regarding the interaction between prestressed reinforcement and sheet piles, the influence of prestress on stress redistribution, and the resulting bearing and deformation behaviors under static loading still require systematic investigation.

Based on the above engineering need and knowledge gap, this study proposes a prestressed geosynthetic reinforced sheet pile retaining wall concept tailored for railway applications. Indoor scaled model tests are conducted to investigate the effects of prestress and pile length on the bearing capacity, horizontal displacement, bending behavior, and reinforcement strain of the wall. The findings aim to elucidate the working mechanism of prestressing in sheet pile–reinforcement–soil systems, provide experimental evidence for structural optimization, and offer new insights for enhancing the performance and reliability of sheet pile retaining walls in modern railway engineering.

2. Experimental setup

2.1 Model design and similarity ratio

According to the industry standards [15] and engineering practice [16], the prototype pile adopts a square cross-section of 1.5 m × 1.5 m, with a center-to-center spacing of 5.875 m. The cantilever segment of the pile is designed to be 6 m, and the embedded segment is 9 m, giving a total length of 15 m. The length ratio between the cantilever and anchored segments of the sheet-pile wall is therefore 1:1.5. The width of the subgrade surface is set to 8.6 m, and the embankment side slope is constructed at 1:1.5.

To minimize scale effects and ensure comparability between the reduced-scale model and the prototype structure, the geometric similarity ratio was determined as 25 based on similarity laws and with reference to the work of Westine et al [17]. For the geosynthetic materials and polyethylene (PE), the test applies corresponding similarity requirements such as dimensions, tensile strength, and elastic modulus. It should be noted that the prototype sheet-pile wall consists of five piles. To facilitate observation of pile displacement and to maintain symmetry, a half-structure model was adopted in the experiment, consisting of two full piles and one half-pile. In addition, the internal dimensions of the model box are 1.4 m × 0.5 m × 1.0 m. The distance between the pile base and the bottom of the box is set to 30 cm (five times the pile width). The four sides of the box are made of high-strength transparent acrylic panels, and the base plate is made of steel, balancing the need to control boundary effects with the requirement for convenient observation.

2.2 Test materials

2.2.1 Sand and polyethylene (PE) sheets

The embankment fill used in the test consists of locally sourced river sand from suburban Chengdu. According to geotechnical testing standards [18], its physical parameters are measured as follows: specific gravity $G_s = 2.6$; characteristic particle sizes d_{10}=0.09 mm,d_{30}=0.3 mm,d_{60}=0.7 mm; uniformity coefficient $C_u = 7.78$; curvature coefficient $C_c = 1.43$; cohesion and internal friction angle $\varphi = 32.6°$. According to the Unified Soil Classification System (USCS), the sand is classified as a well-graded soil. Polyethylene (PE) sheets were used as the material for the piles and facing panels. The elastic modulus obtained from a three-point bending test is 1.32 GPa, which satisfies the similarity requirements.

2.2.2 Geosynthetic Reinforcement Materials

In this test, a nylon mesh with relatively low tensile stiffness was selected as the geosynthetic reinforcement. Tensile performance was evaluated using a universal testing machine in accordance with ASTM D4595-17 [19]. The results show that the tensile strength of the nylon mesh is 10.6 kN/m, the initial (tangent) tensile stiffness reaches 79.19 kN/m, and the elongation at break is 12.83%.

2.3 Test procedure

2.3.1 Model making

The model preparation followed the procedures below: (1) Before filling, the inner surfaces of the model box were cleaned to reduce boundary effects, and the embankment profile and sheet-pile wall positioning lines were marked; (2) Oven-dried river sand was mixed to a moisture content of 10.8%, placed in layers and compacted, with each layer being 5 cm thick, until the elevation of the embankment toe was reached; (3) Earth pressure cells were embedded once the designated elevation was achieved, with the smooth surface facing upward and the cables arranged in an S-shaped pattern; (4) During soil placement around the piles, the compaction effort was controlled to ensure vertical alignment of the piles while maintaining adequate density; (5) The embankment was filled to meet the required geometric dimensions and compaction specifications, and the surface levelness was checked after completion; (6) For the installation of reinforcement layers, the soil surface was leveled, the reinforcement, load-transfer bar, and sheet-pile wall were connected, and filling was continued after fixing; (7) After filling was completed, displacement sensors were installed, the surface was covered with plastic film, and the model was left to stabilize at room temperature for 24 hours.

The sensor placement details are as follows: earth pressure sensors were symmetrically installed on both sides of the central pile and behind the panel, with a vertical spacing of 100 mm; strain gauges were attached to the piles and reinforcement at intervals of 100 mm to monitor strain distribution and bending moment variation. Considering that the central pile is less disturbed than the edge piles, displacement sensors with a measuring range of 30 mm and an accuracy of 0.01 mm were installed at the top and mid-height of the cantilever segment of the central pile. The specific layout of the sensors is shown in Figure 1.

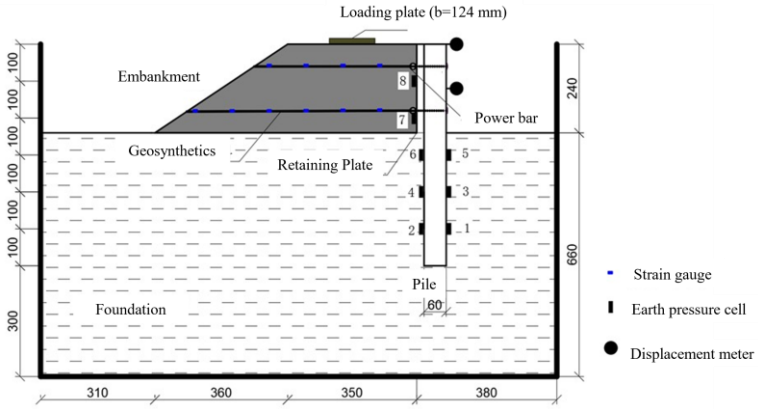

Figure 1. Layout diagram of sensors.

2.3.2 Load application

To investigate the bearing capacity and deformation characteristics of prestressed geosynthetic-reinforced sheet-pile retaining walls, and to analyze the influence of pile length, two sets of indoor scaled model tests were conducted. In Test 1 and Test 2, the pile lengths were 600 mm and 528 mm, respectively, while all other parameters were kept constant: the pile cross-section was 60 mm × 60 mm, and the pile spacing was 235 mm. The load was applied to the embankment surface using a hydraulic actuator, and a loading plate with a width of 124 mm and a thickness of 20 mm was used to simulate the 3.1-m-wide distributed load in the prototype.

The tests consisted of two stages: the pre-prestressed stage and the post-prestressed stage. Prestress was introduced by preloading the reinforced soil, thereby simulating the prestressing effect and establishing a baseline for subsequent performance comparison. The loading rate was controlled at 0.1 mm/min. Loading was terminated when the displacement of the loading plate reached 0.1 times its width (i.e., 12.4 mm). The load corresponding to this displacement was defined as the ultimate bearing capacity of the structure.

3. Results and discussions

3.1 Load-settlement relationship

Figure 2 presents the load–settlement curves of the two tests during the pre-prestressed phase and the post-prestressed phase. It can be observed that, in the early stage of the pre-prestressed phase, the initial slopes of the two curves are nearly identical. This indicates that under low load levels, the external load is primarily carried by the embankment fill, and the additional stress transferred to the reinforcement and the sheet-pile wall is minimal; therefore, the different structural configurations do not yet exhibit noticeable performance differences. When the settlement reaches approximately 4 mm, the load carried in Test 2 becomes lower than that in Test 1. This is attributed to the shorter pile length in Test 2, which provides reduced anchorage capacity, resulting in increased lateral soil displacement and a corresponding decrease in bearing capacity.

At the end of the pre-prestressed phase, the ultimate bearing capacities of Test 1 and Test 2 are 202.068 kPa and 187.048 kPa, respectively, with Test 2 showing a 7.4% reduction relative to Test 1. During the post-prestressed phase, the ultimate bearing capacities increase further due to the compaction effect induced by preloading. The ultimate bearing capacity of Test 1 rises to 245.849 kPa, while that of Test 2 reaches 215.05 kPa, representing increases of 21.7% and 15% relative to the pre-prestressed phase. This improvement is primarily attributed to the “prestress” effect, which

enhances soil compaction, increases the elastic modulus, and improves reinforcement–soil interaction, thereby significantly strengthening the overall bearing performance.

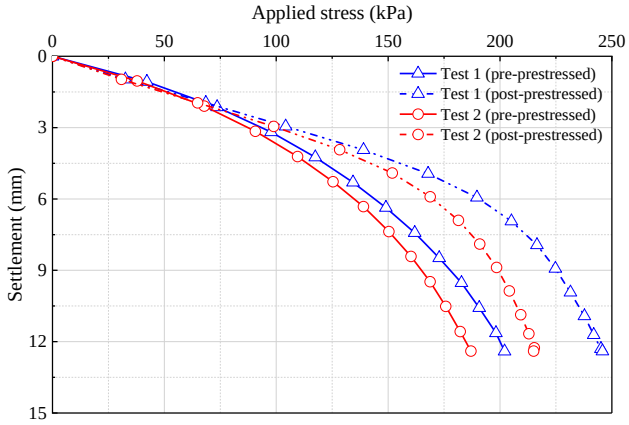

Figure 2. Load-settlement curves of the pile.

3.2 Pile horizontal displacement

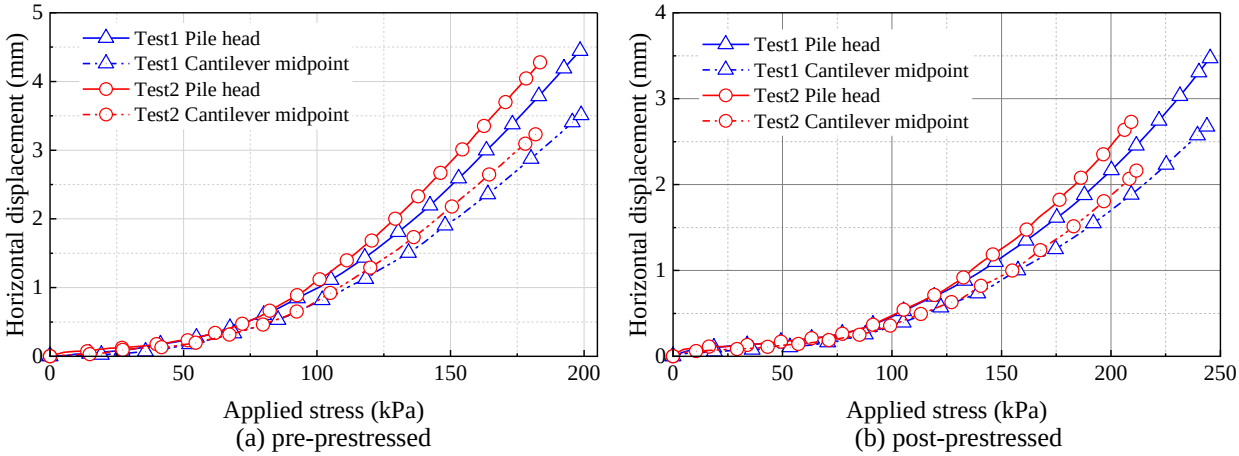

Figure 3. Horizontal displacement of the pile.

Figure 3 illustrates the horizontal displacement curves of the piles in the two tests at different loading stages, including the pile head and the cantilever midpoint. During the preloading (pre-prestressed) phase, the horizontal displacements of both the pile head and the cantilever midpoint in the two tests increase consistently with the applied load. However, the displacement in the short-pile condition (Test 2) is consistently larger than that in the long-pile condition (Test 1). At a load of 180 kPa, the horizontal displacement at the pile head in Test 2 is 4.12 mm, which is 12.5% greater than that in Test 1 (3.67 mm); the displacement at the cantilever midpoint is 3.14 mm, representing a 9.4% increase over Test 1 (2.87 mm). At the ultimate load, the pile-head and cantilever-segment displacements in Test 2 are 4.33 mm and 3.32 mm, respectively. During the post-prestressed (second loading) phase, the pile-head displacement of Test 2 under a load of 180 kPa is 1.95 mm, and the displacement at the cantilever midpoint is 1.48 mm—representing reductions of 52.7% and 52.9%, respectively, compared with the corresponding values in the preloading phase. However, relative to Test 1 in the same phase, the displacements in Test 2 remain 16.7% and 13.8% higher. When the load increases to 210 kPa, the pile-head displacement of Test 2

reaches 2.13 mm, which is still approximately 17.6% greater than that of Test 1 (2.8 mm). These results indicate that reducing pile length weakens the structural restraint capacity, leading to significantly increased horizontal displacement. Meanwhile, the stiffness enhancement induced by the preloading history suppresses subsequent displacement development to a certain extent.

3.3 Horizontal earth pressure

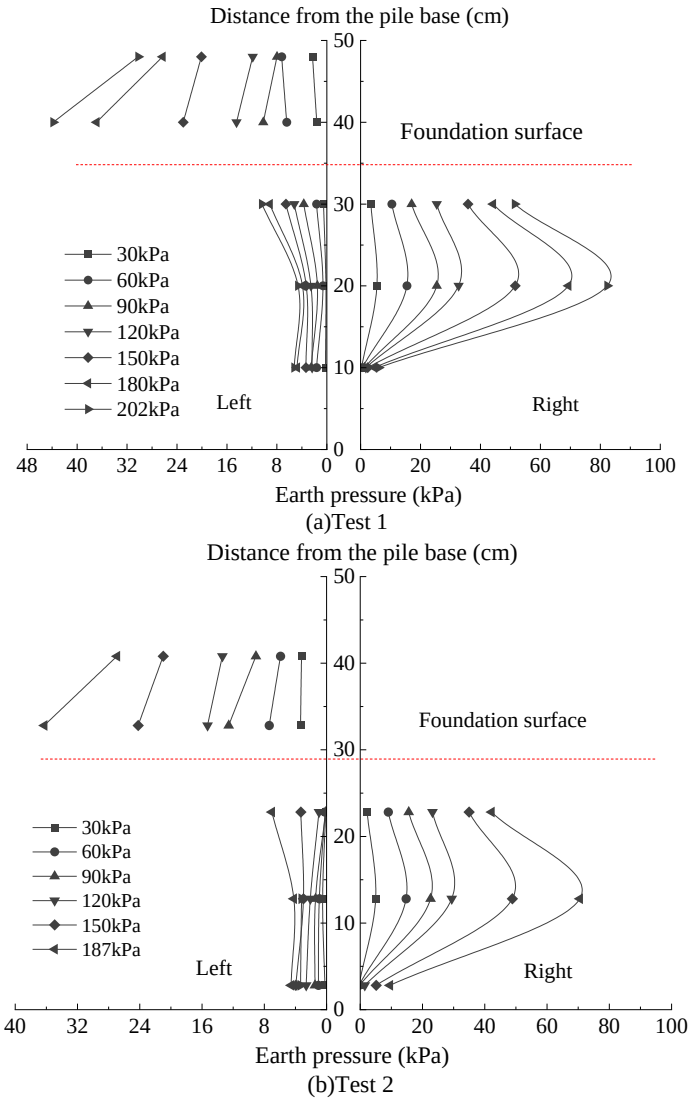

Figure 4. Distribution of horizontal earth pressure on the sheet pile wall at the pre-prestressed phase.

Figures 4 and 5 present the horizontal earth pressure distributions of the sheet-pile wall system for the two tests during the pre-prestressed phase and the post-prestressed phase, respectively. In each figure, the upper-left panel shows the horizontal earth pressure behind the facing panel, while the lower-left and lower-right panels show the horizontal earth pressures on the left and right sides of the pile, respectively. In the pre-prestressed phase, the peak horizontal earth pressure in both tests appears on the right side of the pile, at a height 20 cm above the pile base. This indicates that under external loading, the pile tends to rotate further toward the right, causing the soil on that side to sustain higher pressures. The earth pressure at this measurement point reaches 51.66 kPa, 69.39 kPa,

and 82.37 kPa under loads of 150 kPa, 180 kPa, and the ultimate load, respectively. The earth pressure at the bottom of the facing panel is consistently greater than that at the mid-height of the panel. This can be attributed to two reasons: (1) As the load increases, the accumulated deformation at the panel bottom is relatively small, resulting in stronger restraint on soil deformation and a reduced ability for earth pressure to dissipate. (2) The external load induces pressure diffusion within the embankment; the bottom of the panel lies within the stress diffusion zone, further increasing the earth pressure at that location.

During the post-prestressed phase (second loading), the maximum earth pressure on the pile again appears on the right side at 20 cm above the pile base. The overall distribution pattern remains largely consistent with that observed in the pre-prestressed phase, indicating that the prestressing process does not alter the fundamental distribution mode of earth pressure along the structure. However, under the same load level, the maximum pile earth pressure during the second loading is higher than that during the first loading. This is because the preloading enhances soil stiffness, increases its horizontal resistance, and suppresses pile displacement, resulting in greater transferred earth pressure borne by the pile. The test results show that pile length has no significant influence on the distribution pattern of horizontal earth pressure.

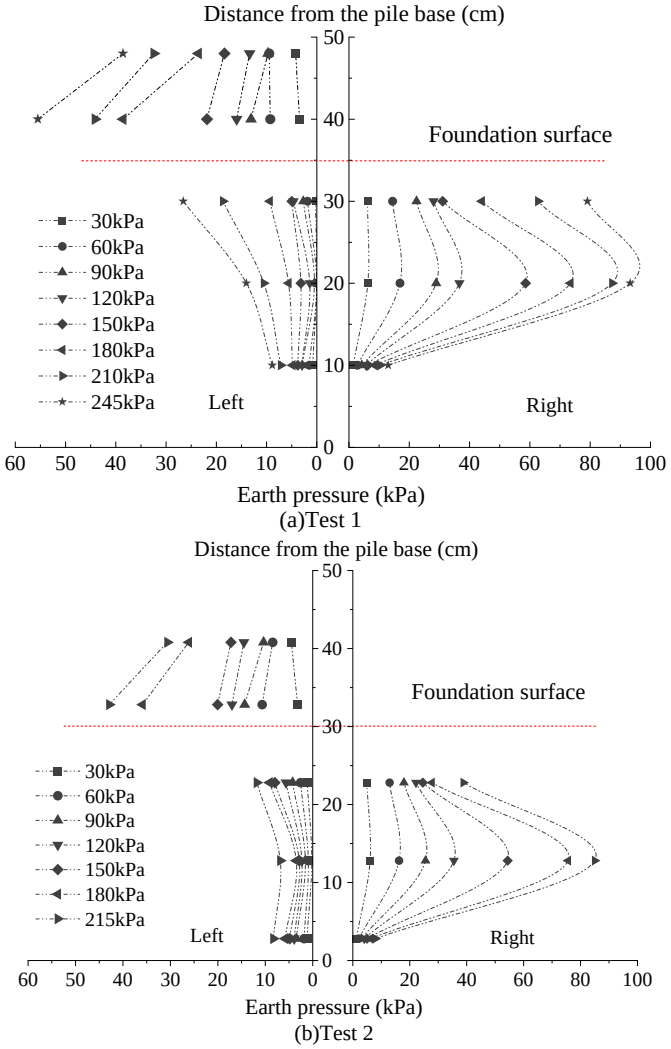

Figure 5. Distribution of horizontal earth pressure on the sheet pile wall at the post-prestressed phase.

3.4 Pile bending moment

In the experiment, strains at the same elevation on both sides of the pile were measured. The bending curvature and bending moment of the pile were then calculated using Equations (1) and (2), as detailed below:

$$\varphi(z) = \frac{\Delta\varepsilon}{a}\# \tag{1}$$

$$M(z) = EI \cdot \varphi(z)\# \tag{2}$$

where z represents the vertical distance from the pile top to the considered location; $\Delta\varepsilon$ is the strain difference between the back and the front surfaces of the pile at that location, measured by the strain gauges; a is the height of the pile segment (0.06 m); and EI is the flexural rigidity of the pile.

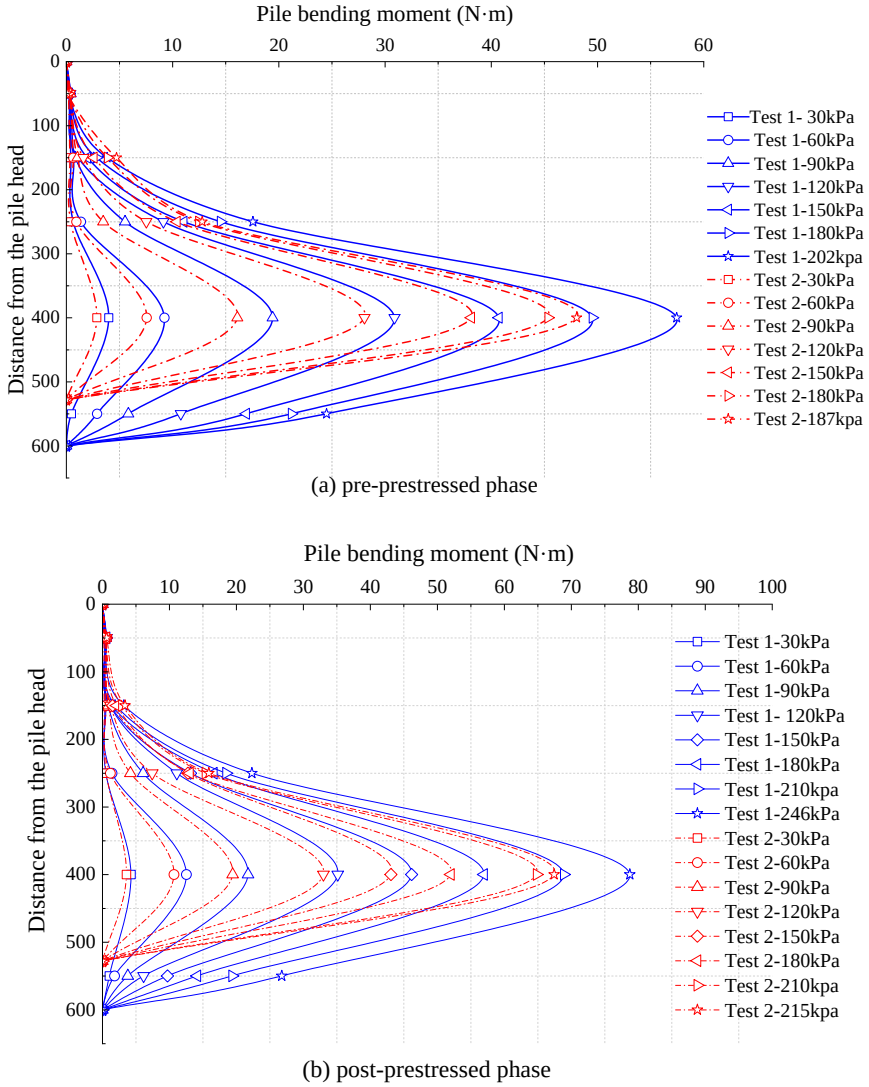

Figure 6. Distribution curves of bending moments in the piles.

Figure 6 presents the pile bending moment distribution curves for the two tests during the pre-prestressed and post-prestressed phases. It can be observed that, in both loading stages, the bending moment along the pile generally increases first and then decreases, with smaller values at

the pile top and bottom, consistent with a parabolic distribution. During the preloading phase, the bending moment in Test 1 begins to increase at 150 mm below the pile top and reaches a peak at a depth of 400 mm (anchored segment), after which it decreases rapidly. As the applied load increases from 30 kPa to 180 kPa, the bending moment at this location rises from 3.99 N ṁ to 49.52 N ṁ, with an ultimate value of 57.47 N ṁ. In the post-prestressed (second loading) phase, the overall distribution remains similar. Within the upper 150 mm of the pile, the bending moment changes gradually due to the distance from the loading plate. At a depth of 400 mm, the bending moment increases from 4.26 N ṁ to 68.90 N ṁ as the load rises, with an ultimate value of 78.76 N ṁ, indicating that second loading under the same applied load produces a larger bending moment.

In Test 2 (shorter pile), the bending moment distribution pattern is similar to that of Test 1, but the magnitudes are generally lower. During the preloading phase, the bending moment at 400 mm depth ranges from 2.87 N ṁ to 45.35 N ṁ, with an ultimate value of 48.05 N ṁ. In the post-prestressed phase, it ranges from 3.58 N ṁ to 64.85 N ṁ, with an ultimate value of 67.45 N ṁ. These results indicate that reducing pile length decreases the bending moment magnitude along the pile but does not alter its overall distribution pattern.

3.5 Reinforcement strain

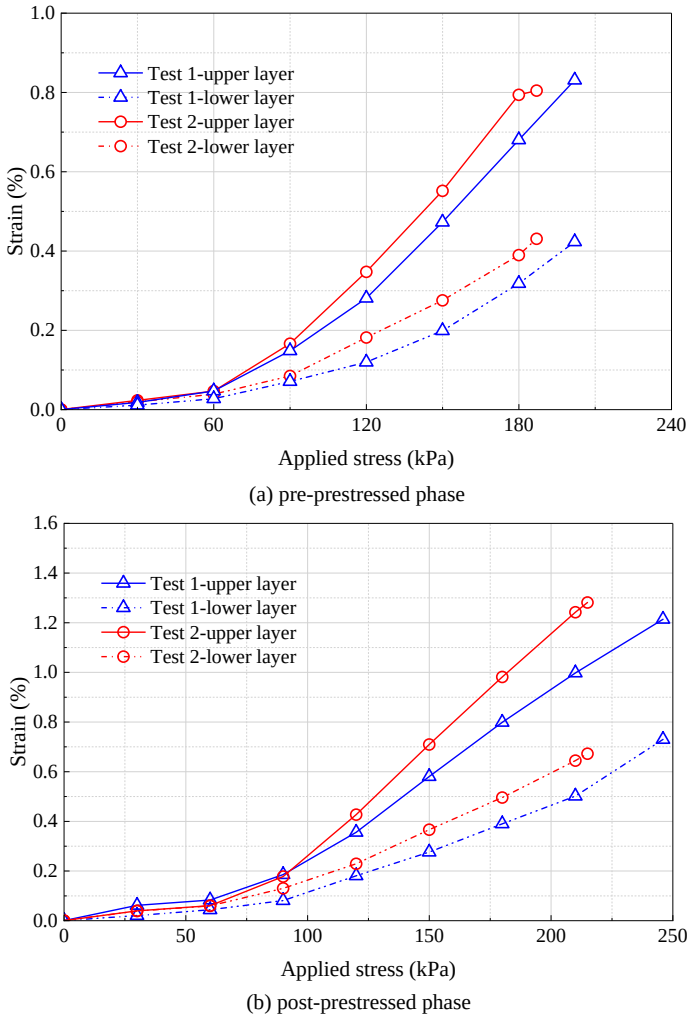

Figure 7. Effect of pile length and prestressing on reinforcement strain.

Figure 7 illustrates the variation of reinforcement strain in the two tests under different preloading stages. Overall, the strain development trends of the reinforcement are similar for both the short- and long-pile conditions: when the applied load is below 30 kPa, strain development is minimal; thereafter, strain increases continuously with increasing load, and the values in the short-pile condition are consistently higher than those in the long-pile condition. During the preloading phase, in the short-pile test, the upper reinforcement strain reaches 0.55% and 0.79% under loads of 150 kPa and 180 kPa, respectively, while the lower reinforcement strain is 0.28% and 0.39%. At the ultimate load, the upper reinforcement strain reaches 0.80%, and the lower strain is 0.43%. In the post-prestressed (second loading) phase, the upper reinforcement strain in the short-pile test increases to 0.71%, 0.98%, and 1.24% under loads of 150 kPa, 180 kPa, and 210 kPa, respectively, while the lower reinforcement strain reaches 0.36%, 0.49%, and 0.64%. At the ultimate state, the upper and lower reinforcement strains are 1.28% and 0.67%, respectively. These results indicate that the prestressing effect also significantly enhances the reinforcement strain in the short-pile test, and under both loading conditions, the short-pile strain is greater than that of the long pile. This is primarily because the ratio of the anchored segment to the cantilever segment in the short pile is 1.2, lower than 1.5 in the long pile, which reduces the restraint capacity of the sheet-pile wall on lateral soil deformation. Consequently, lateral displacement increases, resulting in higher reinforcement strain.

4. Conclusions

This study investigated the bearing capacity and deformation characteristics of prestressed geosynthetic-reinforced sheet-pile retaining walls through two sets of scaled model tests, focusing on the effects of pile length and prestressing. The key findings are as follows:

(1) Prestressing significantly improves the ultimate bearing capacity of the composite wall. Preloading enhances soil compaction, increases the elastic modulus, and strengthens reinforcement–soil interaction, resulting in increases of up to 21.7% in ultimate load compared to the pre-prestressed phase. Shorter piles exhibit reduced bearing capacity due to limited anchorage and increased lateral soil displacement.

(2) Shorter piles lead to higher horizontal displacements and slightly increased earth pressures, reflecting weaker structural restraint. Prestressing effectively suppresses lateral displacement, while the distribution pattern of horizontal earth pressure along the structure remains largely unchanged under different loading stages.

(3) Bending moment distributions along the piles follow a parabolic trend, with maximum values occurring in the anchored segment. Shorter piles result in lower bending moments but similar distribution patterns. Prestressing increases both bending moments and reinforcement strains, particularly in short-pile conditions, highlighting the beneficial influence of preloading on structural stiffness and soil–structure interaction.

Declaration of Competing Interest

The authors declare that they have no known competing financial interests or personal relationships that could have appeared to influence the work reported in this paper.

Acknowledgements

This study is supported by the research grant provided by china railway eryuan chongqing survey and design institute co., ltd.

References

[1] *Al-Refeai TO. Behavior of granular soils reinforced with discrete randomly oriented inclusions. Geotext Geomembr 1991; 10: 319–33.*

[2] *Bosscher Peter J., Gray Donald H. Soil arching in sandy slopes. J Geotech Eng 1986; 112: 626–45.*

[3] *Jamshidi R, Towhata I, Ghiassian H, Tabarsa AR. Experimental evaluation of dynamic deformation characteristics of sheet pile retaining walls with fiber reinforced backfill. Soil Dyn Earthq Eng 2010; 30: 438–46.*

[4] *Bao N, Chen J, Wang G, Sun R, Yan K. Experimental and numerical investigations of seismic behavior of slopes reinforced with sheet pile walls: role of retaining sheet. Eng Geol 2025; 354: 108200.*

[5] *Bransby PL, Milligan GWE. Soil deformations near cantilever sheet pile walls. Géotechnique 1975; 25: 175–95.*

[6] *Gopal Madabhushi S. P., Chandrasekaran V. S. Rotation of cantilever sheet pile walls. J Geotech Geoenvironmental Eng 2005; 131: 202–12.*

[7] *Tatsuoka F, Tateyama M, Mohri Y, Matsushima K. Remedial treatment of soil structures using geosynthetic-reinforcing technology. Geotext Geomembr 2007; 25: 204–20.*

[8] *Wu JTH. Characteristics of geosynthetic reinforced soil (GRS) walls: an overview of field-scale experiments and analytical studies. Transp Infrastruct Geotechnol 2019; 6: 138–63.*

[9] *Zhu Y, Zhang F, Jia S. Embodied energy and carbon emissions analysis of geosynthetic reinforced soil structures. J Clean Prod 2022; 370: 133510.*

[10] *Kumar Shukla S, Chandra S. The effect of prestressing on the settlement characteristics of geosynthetic-reinforced soil. Geotext Geomembr 1994; 13: 531–43.*

[11] *Ma S, Lu L, Wang Z, Xiao L, Arai K. Deflection deformation performance of prestressed geosynthetic-reinforced embankment under differential settlements. Arab J Geosci 2022; 15: 1541.*

[12] *Shivashankar R, Jayaraj J. Behaviour of prestressed geosynthetic reinforced granular beds overlying weak soil. Indian Geotech J 2014; 44: 26–38.*

[13] *Lackner C, Bergado DT, Semprich S. Prestressed reinforced soil by geosynthetics – concept and experimental investigations. Geotext Geomembr 2013; 37: 109–23.*

[14] *Liu C-N, Yang K-H, Nguyen MD. Behavior of geogrid–reinforced sand and effect of reinforcement anchorage in large-scale plane strain compression. Geotext Geomembr 2014; 42: 479–93.*

[15] *Zhao X, Yang Q, Rao J, Geng D, Tan Z. Study of mutual improvement of completed weathered phyllite and red clay based on neutralization effects of swelling and shrinkage deformation 2022: 203–18.*

[16] *Zhao W, Liu X, Xu J, Zhang K. Field monitoring of a composite retaining structure: new sheet pile wall with existing embankment cantilever wall. Geotech Geol Eng 2025; 43: 491.*

[17] *Westine PS, Dodge FT, Baker W. Similarity methods in engineering dynamics: theory and practice of scale modeling. Elsevier; 2012.*

[18] *Germaine JT, Germaine AV. Geotechnical laboratory measurements for engineers. John Wiley & Sons; 2009.*

[19] *Shirazi MG, A Rashid AS, Nazir RB, Abdul Rashid AH, Kassim A, Horpibulsuk S. Investigation of tensile strength on alkaline treated and untreated kenaf geotextile under dry and wet conditions. Geotext Geomembr 2019; 47: 522–9.*